

# Factor-guided functional PCA for high-dimensional functional data

Shoudao Wen and Huazhen Lin\*

Center of Statistical Research and School of Statistics,  
Southwestern University of Finance and Economics

November 23, 2022

## Abstract

The literature on high-dimensional functional data focuses on either the dependence over time or the correlation among functional variables. In this paper, we propose a factor-guided functional principal component analysis (FaFPCA) method to consider both temporal dependence and correlation of variables so that the extracted features are as sufficient as possible. In particular, we use a factor process to consider the correlation among high-dimensional functional variables and then apply functional principal component analysis (FPCA) to the factor processes to address the dependence over time. Furthermore, to solve the computational problem arising from triple-infinite dimensions, we creatively build some moment equations to estimate loading, scores and eigenfunctions in closed form without rotation. Theoretically, we establish the asymptotical properties of the proposed estimator. Extensive simulation studies demonstrate that our proposed method outperforms other competitors in terms of accuracy and computational cost. The proposed method is applied to analyze the Alzheimer's Disease Neuroimaging Initiative (ADNI) dataset, resulting in higher prediction accuracy and 41 important ROIs that are associated with Alzheimer's disease, 23 of which have been confirmed by the literature.

*Key words and phrases:* High-dimensional functional data; factor analysis; factor-guided FPCA; spline approximation; eigenvalue decomposition

---

\*Corresponding author. Email: linhz@swufe.edu.cn. The research were partially supported by National Natural Science Foundation of China (Nos. 11931014 and 11829101).

# 1 Introduction

Advances in technology have enabled us to collect an increasing amount of high-dimensional functional-type data in areas such as medicine, economics, finance, traffic and climatology. Some of these datasets include the Wharton Research Data Services (WRDS) dataset; the Surveillance, Epidemiology, and End Results (SEER) dataset; the Alzheimer’s Disease Neuroimaging Initiative (ADNI) dataset (Mueller et al., 2005) and so on. Since the seminal work of Ramsay (1982), great attention has been given to functional data analysis (FDA); for example, the monographs by Ramsay and Silverman (2002, 2005); Ferraty and Vieu (2006); Horváth and Kokoszka (2012); Hsing and Eubank (2015); Kokoszka and Reimherr (2017). Due to the infinite dimensions of functional data, the compression and dimension reduction of functional data are crucial, in which a popular and powerful tool is functional principal component analysis (FPCA). FPCA takes advantage of the dependence over time and allows us to compress information without much loss. The conventional FPCA approach, termed uFPCA, was proposed for analyzing univariate functional data (Rice and Silverman, 1991; James et al., 2000; Yao et al., 2005; Hall et al., 2008; Li and Hsing, 2010; Zhou et al., 2018; Zhong et al., 2021). When multivariate functional data of  $p$ -dimension is available, Panaretos et al. (2010), Lian (2013), Chiou and Müller (2014), Zhu et al. (2016), Grith et al. (2018) and Han et al. (2018) applied uFPCA to each of them. Since the eigenfunctions and principal component scores of each curve are estimated independently, the dependence among the  $p$  curves is easily ignored by them. Multivariate FPCA (mFPCA) hence was introduced by applying the same scores to each component of multivariate curves so that the dependence among the curves could be taken into account (Ramsay and Silverman, 2005; Chiou et al., 2014; Jacques and Preda, 2014; Górecki et al., 2018; Happ and Greven, 2018; Happ et al., 2019; Wong et al., 2019).

However, it is challenging to extend mFPCA to high-dimensional functional data. First, in mFPCA, because each curve has its own eigenfunctions or principal components, intensive computation is required for high-dimensional functional data. Second, mFPCA expresses all the curves by the same score vector, which may be insufficient to represent features in high-dimensional functional data, and then further analysis based on the obtained scores is also inadequate. Finally, the theory developed for fixed-dimensional mFPCA is not applicable to high-dimensional functional data.

Some studies have considered high-dimensional functional data, and can be roughly divided into three categories: the frameworks of uFPCA (uFPCA-HD), sparse FPCA (sFPCA-HD) and factor models (FM-HD). uFPCA-HD applies uFPCA to each functional variable for a score matrix with a low-rank structure (Gao et al., 2019; Chang et al., 2020; Guo and Qiao, 2020; Solea and Dette, 2021; Fang et al., 2021; Tang and Shi, 2021; Tang et al., 2021). However, since the extracted scores represent the most important features of each functional variable, the information about the correlation among the functional variables is prone to be ignored. Hu and Yao (2022) proposed sparse FPCA by assuming that only a small number of the high-dimensional functional variables have energies. This assumption usually does not hold since the correlation, which is essential for high-dimensional variables, may cause the difficulty of identifying functions with zero or small energies. On the other hand, the FM-HD emphasizes the correlation among  $p$  functional variables. Particularly, Hu and Yao (2021) proposed dynamic principal component analysis (DPCA) based on standard factor analysis at each time point. Tavakoli et al. (2021) and Guo et al. (2022) directly extended the factor model from high-dimensional vector to high-dimensional functional data by regarding functional data as elements in Hilbert space. Hence, the dependence structure over time might be largely ignored by FM-HD. These concerns are also confirmed in Figure 1, which shows that FM-HD performs better, but sFPCA-HD and uPFPCA-HD worsen when the functional variables become correlated; how-

ever, the opposite phenomenon occurs when the dependence over time becomes stronger.

In this paper, we introduce a factor-guided FPCA (FaFPCA) approach to utilize the dependence both over time and among functional variables so that the extracted features from high-dimensional functional data are sufficient. Specifically, we firstly propose factor processes to organize the correlation of functional variables, and then apply uFPCA to each component of the factor processes to address the dependence over time. Although the idea is quite natural, it makes remarkable difference with the existing methods. For example, due to the correlation among functional variables, uFPCA-HD may extract a large number of duplicate features, while ignore some features associated with correlation information among variables because of the first applying FPCA to each functional variable. In contrast, by firstly utilizing factor processes, the proposed FaFPCA efficiently organize the correlation information and avoid overlapping features. Moreover, with applying FPCA to the extracted factor processes, FaFPCA imposes a low-rank structure on the loading function of FM-HD, further captures the information of temporal dependence, and hence is more efficient than FM-HD for dimension reduction.

However, the proposed strategy incurs complicated computations due to the triple-infinite dimension, i.e., the  $\mathbf{B}$  loadings, the  $\boldsymbol{\zeta}$  scores and the  $\boldsymbol{\Phi}(\cdot)$  eigenfunctions are infinite with  $\boldsymbol{\Phi}(\cdot)$  containing  $K \times q$  functions, where  $K \rightarrow \infty$ . A possible estimate method is to iterate among three unknown terms. The computation is intensive and more problematic, the iteration usually fails to converge without appropriate initial values, which are almost impossible to obtain in the current case. In this paper, on the basis of the proposed model and identification conditions, we creatively build some moment equations upon which we estimate  $\mathbf{B}$ ,  $\boldsymbol{\zeta}$  and  $\boldsymbol{\Phi}(\cdot)$  in closed form without rotation. Furthermore, the theoretical properties of the proposed estimator, including the convergence rate and asymptotical normality, are established. The theoretical results suggest that the high dimension  $p$  is a blessing of dimensionality instead of a curse, and both the controlled complexity of

functional data and the limited number of eigenfunctions can significantly improve the estimation accuracy. These findings highlight the importance of using the dependence both over time and among functional variables. Finally, we apply the proposed method to analyze the dataset from ADNI and obtain a higher prediction accuracy than the state-of-the-art methods for high dimensional functional data, such as uFPCA-HD, sFPCA-HD and FM-HD (Gao et al., 2019; Hu and Yao, 2021, 2022; Tavakoli et al., 2021), see Figure 4. Moreover, based on the proposed FaFPCA approach, we identify the atrophy of 41 out of 90 ROIs that are significantly associated with Alzheimer’s disease, where 23 ROIs have been verified by the literature.

The rest of the paper is organized as follows. In Section 2, we introduce the FaFPCA and the estimate method. In Section 3, we establish the main theoretical results. The performance of the proposed estimation procedure is evaluated through simulation studies and real data analyses in Sections 4 and 5, respectively. A brief discussion about further research is given in Section 6. All proofs are detailed in the Supplementary Materials section. The FaFPCA R package based on our method is available on our GitHub home page.

## 2 Model and Estimation

### 2.1 FaFPCA Model

Suppose that the observations  $\mathbf{X}_i(t), i = 1, \dots, n$  are independent identically distributed (iid), with  $\mathbf{X}_i(t) = (X_{i1}(t), \dots, X_{ip}(t))'$  being the high-dimensional functional variables for  $p \gg n$ . For simplicity, we assume that the mean of  $X_{ij}(t)$  has already been removed; namely,  $\mathbb{E}(X_{ij}(t)) = 0$  for any  $j$  and  $t \in [0, 1]$ . To reflect the situation of irregular and possibly subject-specific time points, we assume that  $\mathbf{X}_i(\cdot)$  are measured at  $\mathbf{t}_i = (t_{i1}, \dots, t_{in_i})'$ .

Illustrated by the idea of the factor analysis (Bai and Ng, 2002; Bai, 2003; Bai and Ng,

2006, 2013; Bai and Liao, 2013), we assume the  $\mathbf{X}_i(t)$  are correlated because they share a vector of factor processes  $\mathbf{h}_i(t)$ . The following model is considered:

$$\mathbf{X}_i(t) = \mathbf{B}\mathbf{h}_i(t) + \mathbf{u}_i(t), \quad (1)$$

where  $\mathbf{h}_i(t) = (h_{i1}(t), \dots, h_{iq}(t))'$  is a  $q$ -dimensional vector of factor processes with  $q \ll p$ ,  $\mathbf{B} = (\mathbf{b}_1, \dots, \mathbf{b}_p)' = (b_{jk})_{p \times q}$  is a deterministic matrix, and  $\mathbf{u}_i(t) = (u_{i1}(t), \dots, u_{ip}(t))'$  denotes measurement error independent of  $\mathbf{h}_i(\cdot)$  with  $\mathbb{E}(u_{ij}(t)) = 0$  and  $\text{var}(u_{ij}(t)) = \sigma^2$ . Furthermore, to consider the dependence of functional data over time, we apply the Kauhunen-Loève expansion (Ash and Gardner, 1975) to the factor process  $h_{ij}(t)$ , and have,

$$h_{ij}(t) = \sum_{k=1}^{\infty} \xi_{ijk} \phi_{jk}(t), \quad (2)$$

where  $\phi_{jk}(t)$  is the  $k$ th orthonormal eigenfunction of the covariance function  $C_j(s, t) = \text{cov}(h_{ij}(s), h_{ij}(t))$  for factor process  $j$ , which satisfies  $\int \phi_{jk}(t) \phi_{jk'}(t) dt = 1$  if  $k = k'$ , and it is 0 otherwise;  $\xi_{ijk}, k = 1, 2, \dots$  are the functional principal component scores for the stochastic process  $h_{ij}(t)$  with  $\mathbb{E}(\xi_{ijk}) = 0$ ,  $\text{var}(\xi_{ijk}) = \rho_{jk}$  and  $\text{cov}(\xi_{ijk}, \xi_{ijk'}) = 0$  if  $k \neq k'$ .  $\rho_{jk}$  is the eigenvalue corresponding to the eigenfunction  $\phi_{jk}(\cdot)$ , with the constraint of  $\rho_{j1} \geq \rho_{j2} \geq \dots > 0$  and  $\sum_{k=1}^{\infty} \rho_{jk} < \infty$  for any  $j = 1, \dots, q$ , which implies that  $\sup_{t \in [0, 1]} \mathbb{E}(\sum_{k=1}^K \xi_{ijk} \phi_{jk}(t) - \sum_{k=1}^{\infty} \xi_{ijk} \phi_{jk}(t))^2 \rightarrow 0$  as  $K \rightarrow \infty$ , we hence suppose that

$$h_{ij}(t) = \sum_{k=1}^K \xi_{ijk} \phi_{jk}(t). \quad (3)$$

Model (3) has been extensively studied in the literature of FPCA for the case when  $K$  is fixed (James et al., 2000; Yao et al., 2005; Hall et al., 2008; Zhou et al., 2018). To improve flexibility, we allow  $K \rightarrow \infty$  (Hall and Hosseini-Nasab, 2006; Kong et al., 2016; Lin et al., 2018). In addition,  $K$  can vary with  $j$ , and we use the same  $K$  for  $j = 1, \dots, q$  for simple

notation.

Let  $\boldsymbol{\zeta}_{ij} = (\xi_{ij1}, \dots, \xi_{ijK})'$ ,  $\boldsymbol{\zeta}_i = (\boldsymbol{\zeta}'_{i1}, \dots, \boldsymbol{\zeta}'_{iq})'$  and  $\boldsymbol{\Phi}(t) = \text{diag}(\boldsymbol{\Phi}_1(t), \dots, \boldsymbol{\Phi}_q(t))$ , where  $\boldsymbol{\Phi}(t)$  is a  $Kq \times q$  block diagonal matrix with block  $j$  being  $\boldsymbol{\Phi}_j(t) = (\phi_{j1}(t), \dots, \phi_{jK}(t))'$ . Combined with the expression in (3), the model in (1) can be written as the following factor-guided functional principal component analysis (FaFPCA) model:

$$\mathbf{X}_i(t) = \mathbf{B}\boldsymbol{\Phi}'(t)\boldsymbol{\zeta}_i + \mathbf{u}_i(t). \quad (4)$$

As mentioned above, model (1) highlights the correlation among the functional variables, and the model (3) expresses the temporal dependence of the functional data. As a result, the proposed FaFPCA model in (4) simultaneously organizes the two kinds of dependence structures so that a simple and sufficient expression for the high-dimensional functional may be obtained. Different from the framework of uFPCA (uFPCA-HD), the proposed FaFPCA utilizes factor processes to extract features from functional variables, hence can efficiently avoid overlapping features and organize the correlation information among functional variables. In addition, compared with the framework of factor models (FM-HD), FaFPCA captures the information of temporal dependence by imposing a low-rank decomposition  $\mathbf{B}\boldsymbol{\Phi}'(t)$  on the loading function in FM-HD, and hence is more structured and efficient than FM-HD for dimension reduction.

Obviously, model (4) is not identifiable. We impose three constraints for identifiability:

(I1)  $p^{-1}\mathbf{B}'\mathbf{B} = \mathbf{I}_q$  and the first nonzero element of each column of  $\mathbf{B}$  is positive.

(I2)  $\boldsymbol{\zeta}'\boldsymbol{\zeta}$  is diagonal with decreasing diagonal entries, where  $\boldsymbol{\zeta} = (\boldsymbol{\zeta}_1, \dots, \boldsymbol{\zeta}_n)'$ .

(I3)  $\int \boldsymbol{\Phi}(t)\boldsymbol{\Phi}(t)'dt = \mathbf{I}_{Kq}$  and  $\phi_{jk}(0) > 0$ .

Conditions (I1) and (I2), which are restrictions on loadings and factors, are commonly used in the literature of factor analysis (Bai and Ng, 2013; Fan et al., 2013; Li et al., 2018; Jiang

et al., 2019; Liu et al., 2022). Condition (I3), which restricts the eigenfunctions, is widely used in the literature of FPCA (James et al., 2000; Yao et al., 2005; Hall et al., 2008; Zhou et al., 2018). We state the identifiability in the following proposition, and its proof is detailed in the Supplementary Materials B.

**Proposition 1.** *Under identification conditions (I1)-(I3) and (A1)-(A4) in Section 3,  $\mathbf{B}$ ,  $\zeta$  and  $\Phi(t)$  are unique as  $n \rightarrow \infty$  and  $p \rightarrow \infty$  for both finite  $K$  and divergent  $K$ .*

## 2.2 Estimation Procedure

The estimation involves three terms  $\mathbf{B}$ ,  $\zeta$  and  $\Phi(\cdot)$ . Although model (4) is a kind of factor model, the existing methods for factor analysis are not feasible for the estimation of model (4) because the matrix-structured data required for factor analysis is not available for functional data due to their individual-specific observation times. A possible method is to iterate among the three terms  $\mathbf{B}$ ,  $\zeta$  and  $\Phi(\cdot)$ , which is considerably computationally intensive because all of them are infinite. Moreover, the iteration usually fails to converge without appropriate initial values, which are almost impossible to obtain in the current situation. Here, we avoid the iteration method and solve the computational problem by building some moment equations. Concretely, we denote the covariance matrices of  $\mathbf{X}_i(t)$  and  $\mathbf{u}_i(t)$  by  $\Sigma_{\mathbf{X}}(t)$  and  $\Sigma_{\mathbf{u}}(t)$ , respectively. Let  $\tilde{\Sigma}_{\mathbf{X}} = \int \Sigma_{\mathbf{X}}(t)dt$ ,  $\tilde{\Sigma}_{\mathbf{u}} = \int \Sigma_{\mathbf{u}}(t)dt$  and  $\Lambda_{\zeta} = \text{diag}(\sum_{k=1}^K \text{var}(\xi_{i1k}), \dots, \sum_{k=1}^K \text{var}(\xi_{iqk}))$ . By calculating the covariance matrix and integrating over  $t$  on both sides of (4), we have

$$\tilde{\Sigma}_{\mathbf{X}} = \mathbf{B}\Lambda_{\zeta}\mathbf{B}' + \tilde{\Sigma}_{\mathbf{u}}, \quad (5)$$

which implies that  $p^{-1/2}\mathbf{B}$  is the eigenvector of  $\tilde{\Sigma}_{\mathbf{X}}$ . Considering the identification condition  $p^{-1}\mathbf{B}'\mathbf{B} = \mathbf{I}_q$ , we estimate  $p^{-1/2}\hat{\mathbf{B}}$  for  $p^{-1/2}\mathbf{B}$  by the orthogonal eigenvectors of the numerical



approximation version of  $\tilde{\Sigma}_{\mathbf{X}}$ ; i.e.,

$$\hat{\mathbf{B}} = p^{1/2} \mathbf{E}_{eigen} \left( n^{-1} \sum_{i=1}^n n_i^{-1} \sum_{l=1}^{n_i} \mathbf{X}_i(t_{il}) \mathbf{X}_i'(t_{il}); q \right), \quad (6)$$

where  $\mathbf{E}_{eigen}(A; q)$  is a matrix composed of the orthogonal eigenvectors corresponding to the  $q$  largest eigenvalues of matrix  $A$ .

Now we consider  $\Phi$  and  $\zeta$ . Without loss of generality, we assume that the support of  $t_{ij}$  is  $[0, 1]$  by proper scaling.  $\mathbf{M}(\cdot) = (M_1(\cdot), \dots, M_{\tau_n}(\cdot))'$  denote a vector of B-spline basis functions on  $[0, 1]$  with  $\tau_n = O(n^v)$ ; then we have  $\phi_{jk}(t) \approx \Theta'_{jk} \mathbf{M}(t)$ . Let  $\Theta_j = (\Theta_{j1}, \dots, \Theta_{jK})' \in \mathbb{R}^{K \times \tau_n}$ . With the B-spline approximation, identification condition (I2) on  $\Phi(\cdot)$  can be written as  $\tau_n^{-1} \Theta_j \Theta_j' = \mathbf{I}_K, j = 1, \dots, q$  and  $\tau_n \int \mathbf{M}(t) \mathbf{M}'(t) dt = \mathbf{I}_{\tau_n}$ . Then by (3), we have

$$h_{ik}(t_{il}) = \Phi'_k(t_{il}) \zeta_{ik} \approx \mathbf{M}'(t_{il}) \Theta'_k \zeta_{ik}. \quad (7)$$

On the other hand, by multiplying  $p^{-1} \mathbf{B}'$  on both sides of (1), we have  $p^{-1} \mathbf{B}' \mathbf{X}_i(t) \approx p^{-1} \mathbf{B}' \mathbf{B} \mathbf{h}_i(t)$ . Since  $p^{-1} \mathbf{B}' \mathbf{B} = \mathbf{I}_q$ , we obtain

$$h_{ik}(t_{il}) \approx p^{-1} \sum_{j=1}^q b_{jk} X_{ij}(t_{il}). \quad (8)$$

Combining (7) and (8), we obtain,

$$p^{-1} \sum_{j=1}^q b_{jk} X_{ij}(t_{il}) \approx \mathbf{M}'(t_{il}) \Theta'_k \zeta_{ik}. \quad (9)$$

Then, multiplying  $\mathbf{M}(t_{il})$  on both sides of (9) and making the summation over the obser-

vation times of individual  $i$ , we have

$$\left\{ \sum_{l=1}^{n_i} \mathbf{M}(t_{il}) \mathbf{M}'(t_{il}) \right\}^{-1} \left\{ \sum_{l=1}^{n_i} \sum_{j=1}^p p^{-1} \mathbf{M}(t_{il}) b_{jk} X_{ij}(t_{il}) \right\} \approx \boldsymbol{\Theta}'_k \boldsymbol{\zeta}_{ik},$$

which is a factor model with response  $\mathbf{w}_{ik} = \left\{ \sum_{l=1}^{n_i} \mathbf{M}(t_{il}) \mathbf{M}'(t_{il}) \right\}^{-1} \left\{ \sum_{l=1}^{n_i} \sum_{j=1}^p p^{-1} \mathbf{M}(t_{il}) \hat{b}_{jk} X_{ij}(t_{il}) \right\}$ , factor  $\boldsymbol{\zeta}_{ik}$  and loading  $\boldsymbol{\Theta}_k$ , where  $\hat{b}_{jk}$  is the estimator from (6). Here  $\mathbf{W}_k = (\mathbf{w}_{1k}, \dots, \mathbf{w}_{nk})' \in \mathbb{R}^{n \times \tau_n}$  and  $\boldsymbol{\zeta}_{[k]} = (\boldsymbol{\zeta}_{1k}, \dots, \boldsymbol{\zeta}_{nk})' \in \mathbb{R}^{n \times K}$ ; hence, we estimate  $(\boldsymbol{\zeta}_{[k]}, \boldsymbol{\Theta}_k)$  by

$$(\hat{\boldsymbol{\zeta}}_{[k]}, \hat{\boldsymbol{\Theta}}_k) = \arg \min_{\boldsymbol{\zeta}_{[k]}, \boldsymbol{\Theta}_k} \left\| \mathbf{W}_k - \boldsymbol{\zeta}_{[k]} \boldsymbol{\Theta}_k \right\|_F^2, \quad (10)$$

with  $\|\cdot\|_F$  being the Frobenius-norm of a matrix. Following Bai and Ng (2013), which states that the factors can be estimated asymptotically by principal component analysis (PCA), we obtain estimators for  $\boldsymbol{\Theta}_k$  and  $\boldsymbol{\zeta}_{[k]}$ , respectively by

$$\hat{\boldsymbol{\Theta}}'_k = \mathbf{E}_{eigen}(\mathbf{W}'_k \mathbf{W}_k; K), \quad (11)$$

$$\hat{\boldsymbol{\zeta}}_{[k]} = \tau_n^{-1/2} \mathbf{W}_k \times \mathbf{E}_{eigen}(\mathbf{W}'_k \mathbf{W}_k; K), \quad (12)$$

for  $k = 1, \dots, q$ . Finally, we estimate  $\phi_{jk}(t)$  by  $\hat{\phi}_{jk}(t) = \hat{\boldsymbol{\Theta}}'_{jk} \mathbf{M}(t)$ .

The estimators (6), (11) and (12) for  $\mathbf{B}$ ,  $\boldsymbol{\Theta}$  and  $\boldsymbol{\zeta}$ , respectively, have closed forms based on eigenvalue decomposition without any rotation, and hence, the computation and programming are very simple.

### 2.3 Determining the number of factors and eigenfunctions

We need to determine the dimension of the factor components  $q$  and the number of eigenfunctions  $K$ . Since we transform the estimation for  $\mathbf{B}$ ,  $\boldsymbol{\zeta}$  and  $\boldsymbol{\Phi}(\cdot)$  to the problem of principal component analysis,  $q$  and  $K$  can be selected by calculating the proportion of variability explained by the principal components (James et al., 2000; Happ and Greven,

2018). Particularly, we choose  $q$  and  $K$  such that

$$\sum_{j=1}^q \lambda_j \left( \sum_{i=1}^n n_i^{-1} \sum_{l=1}^{n_i} \mathbf{X}_i(t_{il}) \mathbf{X}_i'(t_{il}) \right) / \sum_{j=1}^p \lambda_j \left( \sum_{i=1}^n n_i^{-1} \sum_{l=1}^{n_i} \mathbf{X}_i(t_{il}) \mathbf{X}_i'(t_{il}) \right) > 95\%,$$

$$\min_{k \in \{1, \dots, q\}} \sum_{j=1}^K \lambda_j(\mathbf{W}'_k \mathbf{W}_k) / \sum_{j=1}^{\tau_n} \lambda_j(\mathbf{W}'_k \mathbf{W}_k) > 95\%,$$

respectively, where  $\lambda_k(A)$  is the  $k$ th eigenvalue of  $A$ . In practice, we can choose a different  $K_k$  for  $k = 1, \dots, q$  so that  $\sum_{j=1}^{K_k} \lambda_j(\mathbf{W}'_k \mathbf{W}_k) / \sum_{j=1}^{\tau_n} \lambda_j(\mathbf{W}'_k \mathbf{W}_k) > 95\%$  is more flexible.

### 3 Theoretical Properties

Let  $K = O(n^\epsilon)$ , the following assumptions are required to establish the theoretical properties of  $\hat{\mathbf{B}}$ ,  $\hat{\boldsymbol{\zeta}}$  and  $\hat{\boldsymbol{\Phi}}(\cdot)$ .

(A1) As  $n \rightarrow \infty$ ,  $\|n^{-1} \boldsymbol{\zeta} \boldsymbol{\zeta}' - \boldsymbol{\Sigma}_\zeta\|_2 \rightarrow 0$  and  $\boldsymbol{\Sigma}_\zeta = \text{diag}(\boldsymbol{\Sigma}_{\zeta,1}, \dots, \boldsymbol{\Sigma}_{\zeta,q})$  is a positive definite diagonal matrix, where  $\boldsymbol{\Sigma}_{\zeta,j} = \text{diag}(\boldsymbol{\Sigma}_{\zeta,j1}, \dots, \boldsymbol{\Sigma}_{\zeta,jK})$ . There exist two positive constants  $C_1, C_2$  such that  $C_1 \leq \sum_{k=1}^K \boldsymbol{\Sigma}_{\zeta,jk} \leq C_2$  for each  $j = 1, \dots, q$ .

(A2) There exist positive constants  $C, a_1, a_2$  and  $C_1, C_2$ , such that (1)  $\sup_j \|\mathbf{b}_j\|_2 \leq C$ ;  
(2) for any  $s > 0$ ,  $P(\sup_{j,k} |\xi_{ijk}| > s) \leq \exp(-(s/C_1)^{a_1})$  and  $P(\sup_j |u_{ij}(t)| > s) \leq \exp(-(s/C_2)^{a_2})$ .

(A3) The random errors  $\mathbf{u}_i(t)$  are independent of each other and  $\boldsymbol{\zeta}_i$ , and  $\mathbb{E}(u_{ij}(t)) = 0$ ,  $\sum_{j'=1}^p |\mathbb{E}[u_{ij}(t)u_{ij'}(t)]| \leq C$  for each  $j$  and uniformly over  $t$ . Furthermore, there exists  $\delta \geq 4$  such that  $\mathbb{E}|p^{-1/2} \sum_{j=1}^p [u_{ij}^2(t) - \mathbb{E}(u_{ij}^2(t))]|^\delta \leq C$  and  $\mathbb{E}\|p^{-1/2} \sum_{j=1}^p \mathbf{b}_j u_{ij}(t)\|_2^\delta \leq C$  uniformly over  $t$ .

(A4)  $p^{-1/2} \sum_{j=1}^p \mathbf{b}_j u_{ij}(t) \xrightarrow{d} N(0, \boldsymbol{\Gamma}(t))$  as  $p \rightarrow \infty$ , where  $\boldsymbol{\Gamma}(t) = \lim_{p \rightarrow \infty} \frac{1}{p} \sum_{j,j'=1}^p \mathbf{b}_j \mathbf{b}'_{j'} \mathbb{E}(u_{ij}(t)u_{ij'}(t))$ .

(A5) Denote that  $w_j$  is the  $j$ -th knot for  $\mathbf{M}(\cdot)$ ,  $\Delta_1 = \max_j |w_j - w_{j-1}|$  and  $\Delta_2 = \min_j |w_j -$

$w_{j-1}|$ . We assume  $\Delta_1 = O(n^{-v})$ , where  $0 < v < 1/2$  and  $\Delta_1/\Delta_2$  is bounded.

(A6)  $\omega = k + s$  for  $k \in \mathbb{N}_+$  and  $s \in (0, 1]$ , and  $\mathcal{H}_\omega = \left\{g(\cdot) : |g^{(k)}(x) - g^{(k)}(y)| \leq C|x - y|^s \text{ for any } x, y\right\}$ . We suppose the true functions  $\{\phi_{jk0} : j = 1, \dots, q; k = 1, \dots, K\} \in \mathcal{H}_r$  with  $r \geq 2$ .

Condition (A1) is commonly used in the factor model (Bai and Ng, 2013) and implies the existence of  $Kq$  factors and the boundedness of corresponding variances. Condition (A2) is similar to Assumption 3.2 in Bai and Liao (2013) for the linear factor model. Particularly, condition (A2.1) requires the loadings to be uniformly bounded, and condition (A2.2) is a requirement on factors and random errors having an exponential tail, which is used to establish the uniform convergence rates of  $\hat{\mathbf{b}}_j$  and  $\hat{\zeta}_i$ . Condition (A3) allows the random errors  $u_{ij}(t)$  to be correlated with each other to some extent. Condition (A4) is a technique condition. Condition (A5) implies that the spline knots are uniform and are commonly used for spline approximation theory. Condition (A6) is a regular smoothing condition on the functions.

**Theorem 1.** *Under Conditions (A1)-(A6), we have*

$$\begin{aligned} \|\hat{\mathbf{b}}_j - \mathbf{b}_{j0}\|_2 &= O_p(\mathcal{R}_{pn}), \\ \sup_j \|\hat{\mathbf{b}}_j - \mathbf{b}_{j0}\|_2 &= O_p((\log p)^{1/2} n^{-1/2} + p^{-1/2}), \end{aligned}$$

for each  $j = 1, \dots, p$ , where  $\mathcal{R}_{pn} = n^{-1/2} + p^{-1/2}$ .

In fact, the convergence rate of  $\hat{\mathbf{b}}_j$  consists of two terms, the estimate error  $\mathcal{R}_{pn}$  and the approximation error  $N_0^{-1/2} = n^{-1/2}(n^{-1} \sum_{i=1}^n 1/n_i)^{1/2}$ , the latter is from the numerical approximation for  $\tilde{\Sigma}_{\mathbf{X}}$  and is ignorable because  $n_i \geq 1$ . The convergence rate in Theorem 1 is similar to those of the linear factor model (Bai and Ng, 2013) and generalized factor model (Liu et al., 2022). According to the results of Theorem 1, we can further establish the asymptotical normality of the loadings.

**Theorem 2.** Under Conditions (A1)-(A6) and when  $np^{-2} = o(1)$ , for each  $j$ , we have

$$\sqrt{n}(\widehat{\mathbf{b}}_j - \mathbf{b}_{j0}) \xrightarrow{d} N(0, \Lambda_\zeta^{-1} \Psi_j \Lambda_\zeta^{-1}),$$

where  $\Psi_j = \mathbb{E} \left[ \left( \int u_{ij}(t) \Phi_0(t) dt \right) \zeta_{i0} \zeta'_{i0} \left( \int \Phi_0(t) u_{ij}(t) dt \right) \right]$  and  $\Lambda_\zeta$  is defined in (5).

A similar asymptotical normality for loadings has also been established in Theorem 2 of Bai (2003), except that  $\Psi_j$  involves integration over time, which comes from the estimation based on (5).

**Theorem 3.** Under Conditions (A1)-(A6), for  $a_1$  defined in Condition (A2) and  $\delta$  defined in Condition (A3), we have

$$\begin{aligned} \|\widehat{\zeta}_i - \zeta_{i0}\|_2 &= O_p \{ \tau_n^{1/2} \mathcal{R}_{pn} + \tau_n^{-r} \} K^{1/2}, \\ \sup_i \|\widehat{\zeta}_i - \zeta_{i0}\|_2 &= O_p \left[ \tau_n^{1/2} \{ (\log n)^{1/a_1} n^{-1/2} + n^{1/2\delta} p^{-1/2} \} + (\log n)^{1/a_1} \tau_n^{-r} \right] K^{1/2}, \end{aligned}$$

for each  $i = 1, \dots, n$ .

Theorem 3 illustrates the samplewise convergence rate of  $\widehat{\zeta}_i$  consisting of two terms, the estimate error  $K^{1/2} \tau_n^{1/2} \mathcal{R}_{pn}$  and approximation error  $K^{1/2} \tau_n^{-r}$ . When  $\tau_n = O(1)$  and  $K = O(1)$ ,  $\Phi(\cdot)$  is specified by finite parameters, so the model (4) is reduced to the traditional factor model and the estimate error becomes  $\mathcal{R}_{pn}$ , which is consistent with the result of Theorem 1 in Bai and Ng (2002). In addition, for finite functions with  $K = O(1)$  and  $n/p \rightarrow 0$ , the error is controlled by the sample size  $n$ ,  $\widehat{\zeta}_i$  reaches the convergence rate of  $n^{-r/(2r+1)}$  after taking  $v = 1/(2r+1)$ . The convergence rate comes from the estimation of finite eigenfunctions and is optimal for nonparametric function estimation (Stone, 1980). Theorem 3 also shows that the uniform convergence rate of  $\widehat{\zeta}_i$  is slower than the samplewise convergence rate. This conclusion is consistent with those for the linear factor model (Bai and Ng, 2013) and generalized factor model (Liu et al., 2022).

In particular, when  $\tau_n = O(1)$  and  $K = O(1)$  for the parametric factor model, the uniform estimate error  $\{(\log n)^{1/a_1} n^{-1/2} + n^{1/2\delta} p^{-1/2}\} \tau_n^{1/2} K^{1/2}$  reduces to  $(\log n)^{1/a_1} n^{-1/2} + n^{1/2\delta} p^{-1/2}$ , which is similar to the uniform rate  $n^{-1/2} + n^{1/2\delta} p^{-1/2}$ , as shown in Theorem 3.1 in [Bai and Liao \(2013\)](#) for the traditional factor model.

**Remark 1.** *To guarantee the samplewise consistency of factors or variablewise consistency of loadings, we require that  $p$  diverges at any rate, including an exponential rate with respect to  $n$ . Our simulation studies show that the performance of the proposed method improves as  $p$  and  $n$  increase. That is, the high dimensional  $p$  is a blessing of dimensionality instead of a curse. This is a direct result of the factor model, where  $p$  actually plays the role of the number of observations for estimating  $\zeta_i$ . In our opinion, more variables provide more information to estimate the models when the factor number or latent freedom is fixed. The issue where the high dimensional  $p$  is a blessing of dimensionality instead of curse has also been well addressed for the linear factor model in [Li et al. \(2018\)](#).*

**Theorem 4.** *Under Conditions (A1)-(A6) for each  $j = 1, \dots, q$ , we have*

$$\sum_{k=1}^K \int \left( \widehat{\phi}_{jk}(t) - \phi_{jk,0}(t) \right)^2 dt = O_p \{ \tau_n \mathcal{R}_{pn}^2 + \tau_n^{-2r} \} K$$

Theorem 4 establishes the convergence rate for eigenfunctions  $\widehat{\mathbf{\Phi}}(t)$ , which consists of two terms, the estimate error  $K^{1/2} \tau_n^{1/2} \mathcal{R}_{pn}$  and approximation error  $K^{1/2} \tau_n^{-r}$ , which is similar to Theorem 3.

## 4 Numerical Studies

In this section, we conduct simulation studies to assess the finite-sampling performance of the proposed method (FaFPCA) by comparing it with state-of-the-art methods, including uFPCA-HD ([Gao et al., 2019](#)), FM-HD ([Tavakoli et al., 2021](#)), sparse functional

principal analysis (sFPCA-HD, [Hu and Yao 2022](#)), dynamic principal component analysis (DPCA, [Hu and Yao 2021](#)) for high-dimensional functional data. The performance of the estimator is evaluated via the computational time and the accuracy of the estimator, including the root mean square error  $\text{RMSE}_l = p^{-1/2} \|\widehat{\mathbf{B}} - \mathbf{B}_0\|_F$  for the loadings,  $\text{RMSE}_f = n^{-1/2} \|\widehat{\boldsymbol{\zeta}} - \boldsymbol{\zeta}_0\|_F$  for the factors,  $\text{RMSE}_e = \|\widehat{\boldsymbol{\Phi}}(t) - \boldsymbol{\Phi}(t)\|_F = \left( \sum_{j,k} \int (\widehat{\phi}_{jk}(t) - \phi_{jk0}(t))^2 dt \right)^{1/2}$  for the eigenfunctions, and normalized prediction error (PE) =  $\sum_{i,j} n_i^{-1} \sum_{l=1}^{n_i} (\widehat{X}_{ij}(t_{il}) - X_{ij}(t_{il}))^2 / \sum_{i,j} n_i^{-1} \sum_{l=1}^{n_i} X_{ij}^2(t_{il})$  for the observations  $X_{ij}(t_{il})$  in the testing set, which is independent of the training data but has the same distribution and size as the training data.

## 4.1 Simulation setting

For each trajectory  $\mathbf{X}_i(t)$ , 20 observation time points are randomly sampled from  $U(0, 10)$  and 200 replicates are applied in each scenario unless otherwise stated.

**Scenario 1:** To be fair, we generate data from the following model, which does not follow the assumptions of the methods we consider,

$$\mathbf{X}_i(t) = \sum_{k=1}^K \boldsymbol{\zeta}_{ik} \phi_k(t) + \boldsymbol{\epsilon}_i(t), \quad i = 1, \dots, n,$$

where  $\boldsymbol{\zeta}_{ik} \in \mathbb{R}^p \sim N(\mathbf{0}, \boldsymbol{\Sigma}_{\boldsymbol{\zeta},k})$ ,  $\boldsymbol{\epsilon}_i(t) \sim N(\mathbf{0}, \boldsymbol{\Sigma})$  for each  $t$ ,  $(\boldsymbol{\Sigma}_{\boldsymbol{\zeta},k})_{ij} = 0.5^{|i-j|}$  if  $i \neq j$  and  $(\boldsymbol{\Sigma}_{\boldsymbol{\zeta},k})_{ii} = 3 - (k-1)/(K-1)$  for each  $i = 1, \dots, p$  and  $k = 1, \dots, K$ . We take  $\boldsymbol{\Sigma} = (\sigma_{ij})_{p \times p}$  as **Case I** :  $\boldsymbol{\Sigma} = \mathbf{I}$  and **Case II** :  $\sigma_{ii} = 1$  and  $\sigma_{ij} = 0.3$  if  $i \neq j$ , and let  $\phi_k(t) = \sin[(2k-1)\pi t/10]$ ,  $n = p = 100$  and  $K = 2, 10$ .

**Scenario 2:** To investigate the performance of the estimation for loadings, factors and eigenfunctions, we generate functional data by  $\mathbf{X}_i(t) = \mathbf{B}\mathbf{h}_i(t) + \mathbf{u}_i(t)$ ,  $i = 1, \dots, n$ , which satisfy the assumption of the proposed method, where random error  $\mathbf{u}_i(t) \sim N(\mathbf{0}, \mathbf{I})$ . To construct  $\mathbf{B}$ , we first generate  $n$  samples of the  $p$ -dimensional  $\mathbf{k}_i$  from  $N(0, (\sigma_{ij})_{p \times p})$  with

$\sigma_{ij} = 0.5^{|i-j|}$ . Here,  $\mathbf{K} = (\mathbf{k}_1, \dots, \mathbf{K})'$ . We apply eigendecomposition to the matrix  $\mathbf{K}\mathbf{K}'$  to obtain  $\mathbf{B}_q$  and  $\mathbf{K}_q$ , where  $\mathbf{B}_q$  is a diagonal matrix whose diagonal entries are the first  $q$  largest eigenvalues of  $\mathbf{K}\mathbf{K}'$ , and  $\mathbf{K}_q \in \mathbb{R}^{n \times q}$  consists of the corresponding eigenvectors.  $\mathbf{B}_n = \mathbf{K}'\mathbf{K}_q$ , and QR decomposition of  $\mathbf{B}_n = \mathbf{Q}_n\mathbf{R}_n$  is performed. Then,  $\mathbf{B} = p^{1/2}\mathbf{Q}_n$  so that the identification condition on  $\mathbf{B}$  can be satisfied. Similarly, to construct  $\zeta_i$  for  $\mathbf{h}_i(t)$ , we independently generate  $\xi_{ik}^* \sim N(0, Kqk^{-1})$ , denote  $\zeta_i^* = (\xi_{i1}^*, \dots, \xi_{i,Kq}^*)'$  and  $\zeta^* = (\zeta_1^*, \dots, \zeta_n^*)$ , and then perform eigen-decomposition of the matrix  $\zeta^*\zeta^{*\prime}$  for matrices  $\mathbf{\Lambda}_{Kq}$  and  $\mathbf{M}_{Kq}$ , which consist of the first  $Kq$  largest eigenvalues and the corresponding eigenvectors, respectively. We take  $\zeta \hat{=} (\zeta_1, \dots, \zeta_n)' = \mathbf{\Lambda}_{Kq}^{1/2}\mathbf{M}'_{Kq}$ . It is easy to check that  $\zeta$  satisfies Identification Condition (I2), as described in Section 2.1. Given  $\zeta_i$ , the factor process  $\mathbf{h}_i(t) = (h_{i1}(t), \dots, h_{iq}(t))'$  is generated by  $h_{ij}(t) = \sum_{k=1}^K \xi_{ijk} \phi_{jk}(t)$ , where  $\phi_{jk}(t) = \sqrt{2} \sin[\{2(j \neq 2) + (j = 2)\}k\pi t/10]$  if  $k$  is odd and  $\phi_{jk}(t) = \sqrt{2} \cos[\{2(j \neq 2)k + (j = 2)(2k + 1)\}\pi t/10]$  if  $k$  is even. The setting is used to ensure the orthogonality of eigenfunctions.

## 4.2 Simulation results

**Scenario 1:** We first compare FaFPCA with the existing methods in terms of prediction accuracy PE. Figure 1 shows the PE of the proposed FaFPCA, FM-HD, DPCA, sFPCA-HD and uPFCA-HD methods with the corresponding optimal tuning parameters under the cases listed in Scenario 1. From Figure 1, we can see that (1) When  $\mathbf{u}_i(t)$  becomes correlated, that is, when  $\mathbf{\Sigma}$  changes from  $\mathbf{I}$  to  $\mathbf{\Sigma} \neq \mathbf{I}$  in Figures 1(a) and 1(b), respectively, FaFPCA, FM-HD, and DPCA perform better, while the PE performance of sFPCA-HD and uPFCA-HD worsens. This indicates that FaFPCA, FM-HD and DPCA are efficient in making use of the correlations among functional variables while sFPCA-HD and uPFCA-HD are not. (2) On the other hand, when  $K$  changes from 10 to 2 in Figures 1(c) and 1(d), which means the dependence over time gets stronger, sFPCA-HD and uPFCA-HD perform better, while FM-HD and DPCA perform worse. This is not surprising because sFPCA-HD



and uPFCA-HD focus on dependence over time while FM-HD and DPCA do not. (3) The proposed FaFPCA approach performs the best and is stable in all the cases in terms of PE; particularly, either the dependence over time or correlations among variables increase, the accuracy of FaFPCA is improved. Compared to the other methods, the obtained by FaFPCA is due to the usage of the two kind of correlations.

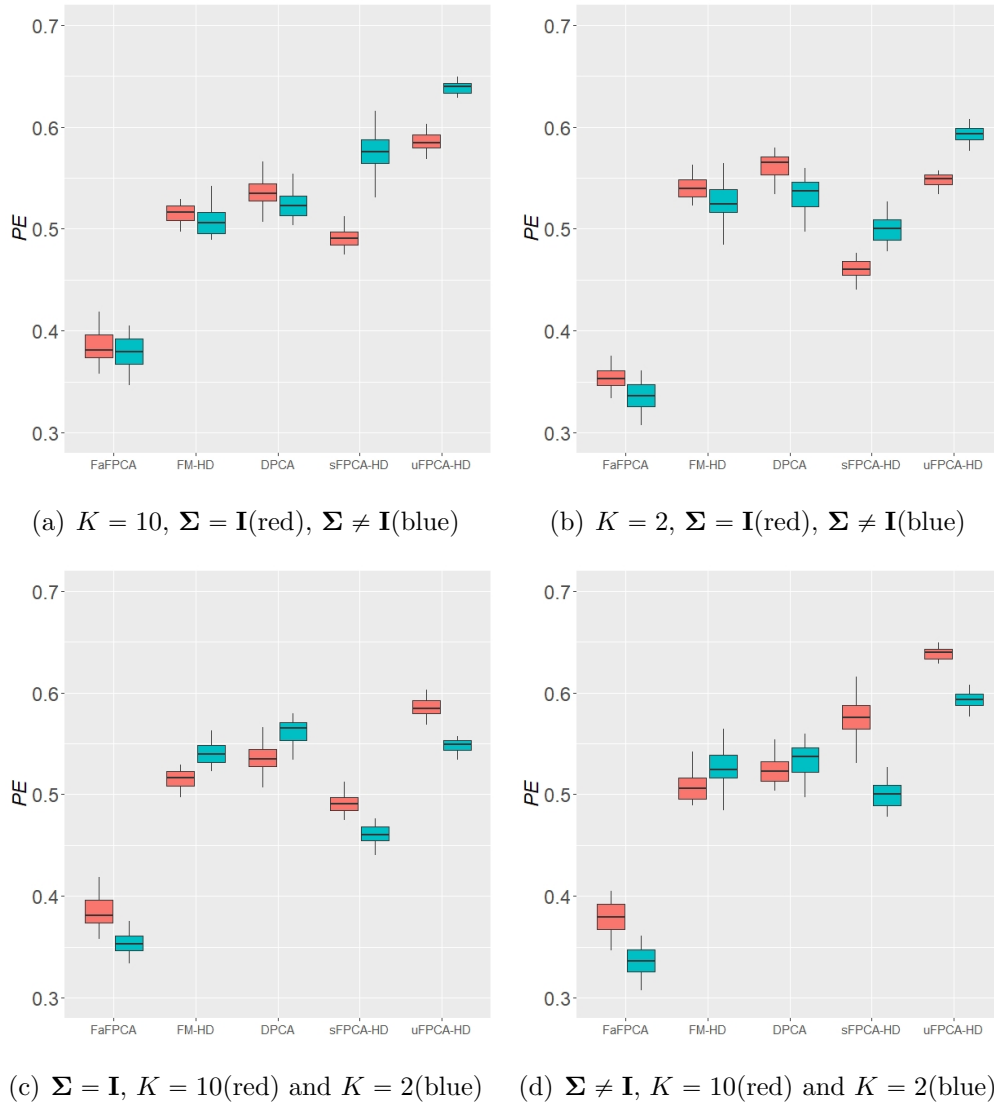


Figure 1: The PEs of the FaFPCA, FM-HD, DPCA, sFPCA-HD and uPFCA-HD methods under the cases listed in Scenario 1.

We carried out the computation on a single 4-core personal laptop with 16 GB of RAM. Table 1 shows the average running time of 200 repetitions for Case I with  $K = 2$ . Table 1 shows that the proposed FaFPCA approach is much faster than the other methods except

FM-HD, which only considers model (1) and does not estimate eigenfunctions and factor scores. uFPCA-HD requires an extremely large amount of time because uFPCA is applied to each of the  $p$  curves separately.

Table 1: The computational time in seconds of the five methods.

|      | FaFPCA | FM-HD  | DPCA   | sFPCA-HD | uFPCA-HD |
|------|--------|--------|--------|----------|----------|
| Mean | 0.0300 | 0.0190 | 0.4570 | 0.2430   | 77.3500  |
| SD   | 0.0097 | 0.0095 | 0.0178 | 0.0283   | 3.0647   |

**Scenario 2:** Figure 2 displays  $RMSE_l$  for loadings,  $RMSE_f$  for factors and  $RMSE_e$  for eigenfunctions using the proposed FaFPCA method for Scenario 2 with  $(q, K) = (5, 2)$  when  $(n, p)$  varies. The results in Figure 2 indicate that the precision of  $\mathbf{B}, \boldsymbol{\zeta}$  and  $\boldsymbol{\Phi}(t)$  increases as  $n$  or  $p$  increases, which is consistent with the theoretical results. In particular, the precision of  $\boldsymbol{\zeta}$  is more sensitive to  $p$  than to  $n$ , while that of  $\mathbf{B}$  is more sensitive to  $n$ . This is because the estimator for  $\boldsymbol{\zeta}_i$  is based on  $p$  functions of individual  $i$ ; however, the estimator for  $\mathbf{B}$  is mainly based on  $n$  individuals.

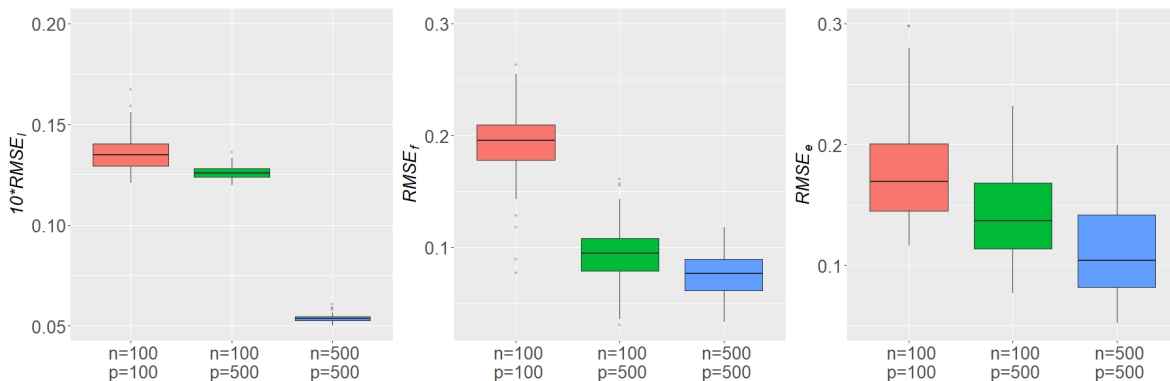


Figure 2: The boxplots of  $10 \times RMSE_l, RMSE_f$  and  $RMSE_e$  (from left to right) of the FaFPCA for Scenario 2 with  $n, p = 100, 500$ . The  $RMSE_l, RMSE_f$  and  $RMSE_e$  are the root of mean square errors for loadings, factors and eigenfunctions, respectively.

To show the effect of the number of observations, we take  $n_i$  from 5 to 50 given  $n = p = 100$  and  $(q, K) = (5, 2)$ . The results in Figure 3 show that the estimators

are quite stable with respect to  $n_i$  except for small  $n_i$  values. When  $n_i$  is small, the matrix  $\sum_{l=1}^{n_i} \mathbf{M}(t_{il})\mathbf{M}'(t_{il})$  in  $\mathbf{w}_{ik}$  might be irreversible. To avoid this problem, we add a term  $\lambda \mathbf{I}_{\tau_n}$ , where  $\lambda$  is small, to  $\sum_{l=1}^{n_i} \mathbf{M}(t_{il})\mathbf{M}'(t_{il})$  to ensure invertibility. This may cause extra bias for the estimations of factors and eigenfunctions when  $n_i$  is small. From Figure 3, we also observe an interesting phenomenon as  $n_i$  increases,  $\text{RMSE}_l$  for loadings increases, while  $\text{RMSE}_f$  and  $\text{RMSE}_e$  for factors and eigenfunctions, respectively, decrease. This can be attributed the following two aspects. On the one hand, the loadings are estimated mainly based on  $n$  samples, rather than  $n_i$  or  $p$ ; hence, the increasing  $n_i$  values may introduce extra noise due to the integration of all observations using (6). On the other hand, the factors  $\zeta_i$  are estimated mainly based on the observations from individual  $i$ ; hence, the estimation of the factors becomes better as  $n_i$  increases, although becomes stable when  $n_i$  is large enough, for example, when  $n_i > 10$  in the cases. The estimation of eigenfunctions has a similar performance as that of the factors since they are simultaneously estimated.

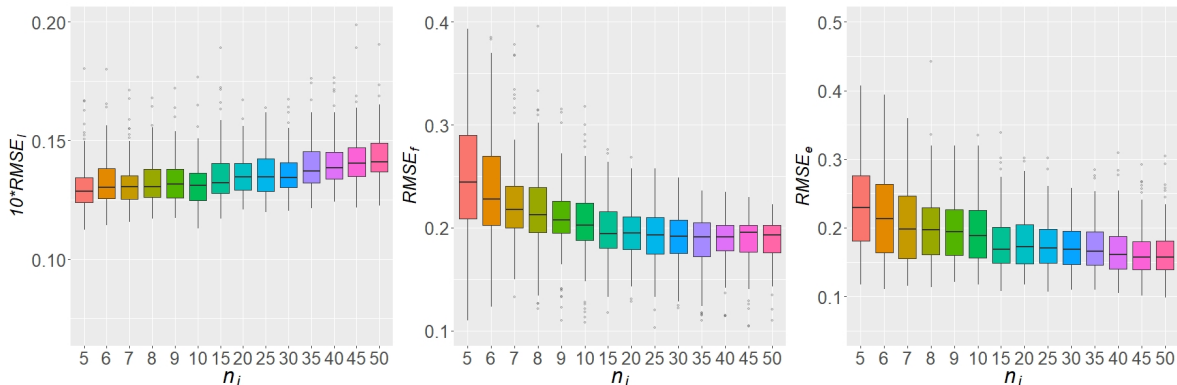


Figure 3: The boxplots of  $10 \times \text{RMSE}_l$ ,  $\text{RMSE}_f$  and  $\text{RMSE}_e$  (from left to right) of the FaFPCA when  $n_i$  changes from 5 to 50. The  $\text{RMSE}_l$ ,  $\text{RMSE}_f$  and  $\text{RMSE}_e$  are the root of mean square errors for loadings, factors and eigenfunctions, respectively.

## 5 Real Data Analysis

Alzheimer's disease (AD) is irreversible and the most common form of dementia, and it can result in the loss of thinking, memory and language skills. It is important to determine the

progress of AD by monitoring alterations in the brain and to detect the disease at an early stage. Particularly, it is well known that the atrophy of the region of interest (ROI) is associated with AD detection and some studies consider local brain volumes for characterizing regional atrophy (Zhao et al., 2019; Zhong et al., 2021; Li et al., 2022). In the paper, we use the brain volume density values within different ROIs to detect the progression of AD. The dataset includes a subset of participants with 766 subjects enrolled in the first phase of the ADNI study (Mueller et al., 2005) with AD, mild cognitive impairment (MCI, an early stage of AD) and cognitively normal (CN). A total of 172, 378 and 216 participants were diagnosed with AD, MCI and CN, respectively. Each participant’s record consists of the brain volume density values of 90 ROIs for each of the 501 equispaced sampling volumes in the interval of  $[-255, 255]$ , so that we can regard the brain volume density as a curve. To be specific, we denote  $\mathbf{X}_i(t)$  by the brain volume density curves of ROIs of the  $i$ -th individual, which are functions of the log of the Jacobian volume (denoted by  $t$ ). We scale the log Jacobian volume into  $[0, 1]$  before analysis and the summary of the ROIs is shown in Table 2. Consequently, 90 ROIs are high-dimensional functional variables that can be analyzed by the proposed FaFPCA approach, as well as the methods mentioned in Section 4 for comparison.

We apply FaFPCA, FM-HD, DPCA, sFPCA-HD and uFPCA-HD to the data without the label information of AD, MCI and CN. First, based on the criteria in Section 2.3, we choose  $q = 5$  factors and  $K = 3$  eigenfunctions for FaFPCA. Similarly, on the grounds of the proportion of variability, we choose  $q = 5$ ,  $K = 15$ ,  $K = 33$  and  $K = 2$  for the FM-HD, DPCA, sFPCA-HD and uFPCA-HD methods, respectively. We randomly set 60% of the dataset as the training set and the other data as the test set with 200 repeats. Figure 4(a) presents the PEs of FaFPCA, FM-HD, DPCA, sFPCA-HD and uFPCA-HD with the corresponding selected hyperparameters and shows that FaFPCA yields the estimator with the highest prediction accuracy. In addition, Figure 4(a) also shows that the sFPCA-HD

and uFPCA-HD methods are the worst in terms of PE, which indicates that the correlation among functional variables might be strong in the ADNI data.

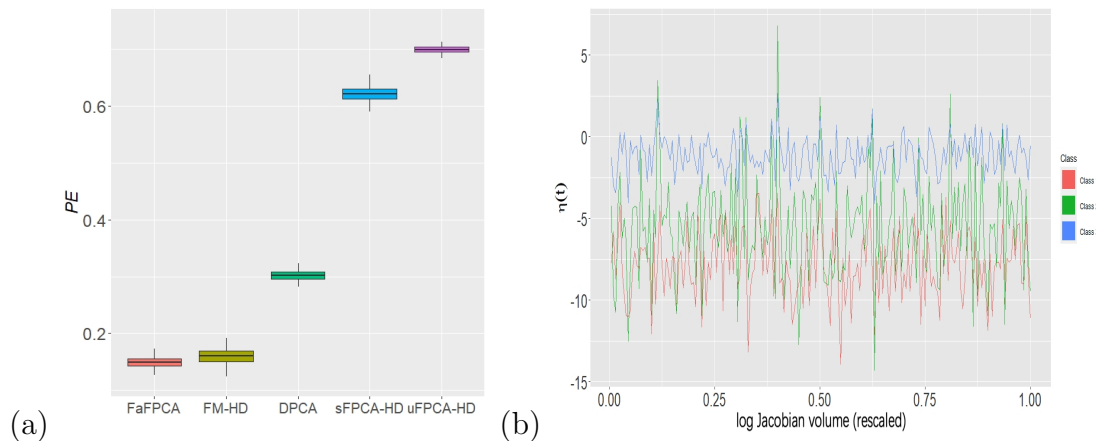


Figure 4: (a) The PEs of FaFPCA, FM-HD, DPCA, sFPCA-HD and uFPCA-HD for the ADNI dataset. (b) The regression coefficient functions of choosed ROIs in each class.

Now, we investigate details about the factors in Figure 5. Based on the top ten largest absolute values of the loadings, factor 1 extracts the feature mainly from variables ROI<sub>12</sub>, ROI<sub>15</sub>, ROI<sub>16</sub>, ROI<sub>51</sub>, ROI<sub>91</sub>, ROI<sub>92</sub>, ROI<sub>631</sub>, ROI<sub>632</sub>, ROI<sub>1016</sub> and ROI<sub>2016</sub>, which represent the information on the brain regions starting from the forebrain, arriving at the base of the brain, and then returning to the afterbrain. These ROIs exist in the bottom lateral part of the brain and mostly in the cerebellum. Factor 2 withdraws the information of variables ROI<sub>5</sub>, ROI<sub>16</sub>, ROI<sub>17</sub>, ROI<sub>18</sub>, ROI<sub>28</sub>, ROI<sub>50</sub>, ROI<sub>53</sub>, ROI<sub>54</sub>, ROI<sub>49</sub> and ROI<sub>60</sub>, which express information on the basal nucleus and are located deeply in the white matter of the brain. Factors 3-5 extract the information from regions similar to those of factor 2.

Since  $q = 5$  is selected, we can use the 5-dimensional vector to represent each ROI, resulting in  $\hat{\mathbf{B}} \in \mathbb{R}^{90 \times 5}$  for 90 ROIs. Then, based on the estimated  $\hat{\mathbf{B}}$ , we cluster the ROIs into 3 classes by  $K$ -means, and the clusters are displayed in Table 2. We can see that class 1 mainly includes the ROIs in the basal nucleus, class 2 mainly contains the ROIs in the junction between the brain and basal nucleus, and class 3 involves the ROIs in the brain, including the lateral and medial parts of the left and right hemispheres.

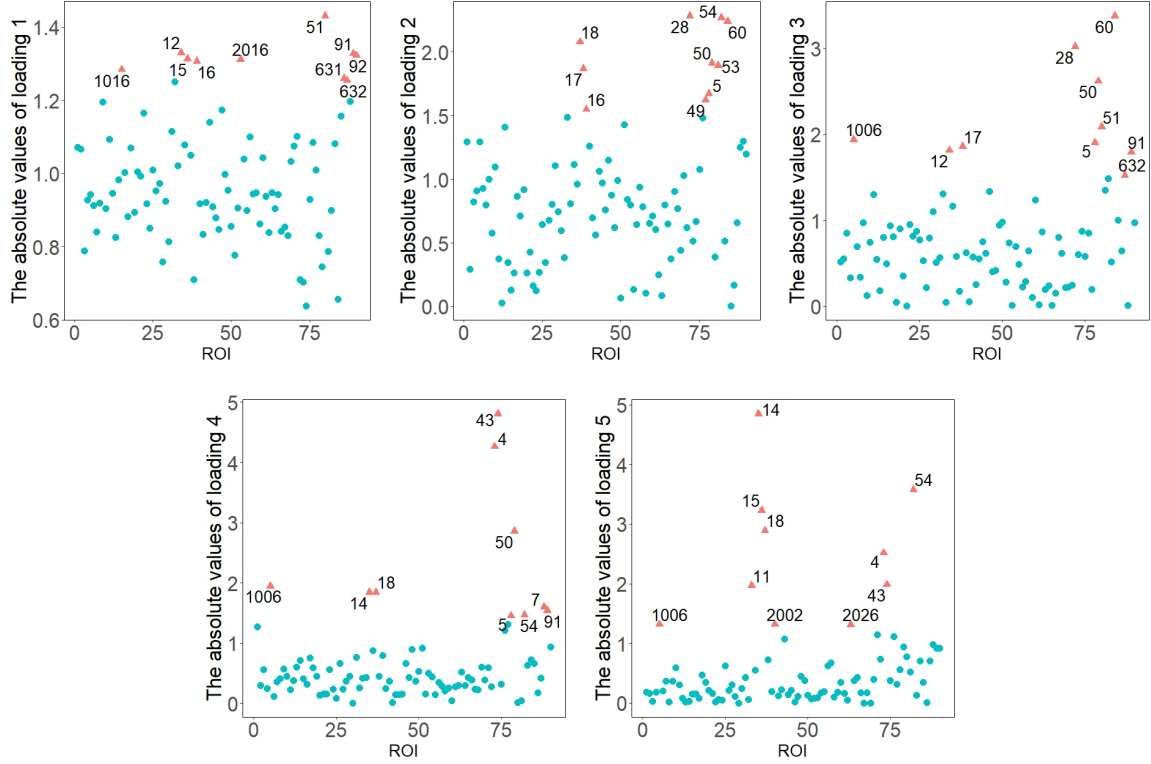


Figure 5: The absolute values of the 5 loadings, where the red triangular dots are the first 10 largest absolute values of loadings.

We also investigate the effects of the ROIs on AD. First, we conduct multivariate logistic regression with AD, MCI and CN as responses and  $\widehat{\zeta}_i$  as covariates. The regression coefficients are denoted by  $\alpha$ . Hence,  $\alpha' \widehat{\zeta}_i$  can be regarded as the measurement of the effect of the ROIs on AD. On the other hand, by multiplying  $p^{-1} \Phi(t) \mathbf{B}'$  on both sides of (4) and coupling it with the identification condition  $p^{-1} \mathbf{B}' \mathbf{B} = \mathbf{I}_q$ , we obtain  $p^{-1} \Phi(t) \mathbf{B}' \mathbf{X}_i(t) \approx \Phi(t) \Phi'(t) \zeta_i$ . After combining it with the identification condition  $\int \Phi(t) \Phi'(t) dt = \mathbf{I}$ , we have

$$p^{-1} \int \alpha' \Phi(t) \mathbf{B}' \mathbf{X}_i(t) dt \approx \alpha' \int \Phi(t) \Phi'(t) dt \zeta_i = \alpha' \zeta_i.$$

Then, the regression relationship  $\alpha' \zeta_i$  between response  $Y_i$  and factor  $\zeta_i$  can be written as  $\int \boldsymbol{\eta}'(t) \mathbf{X}_i(t) dt$  between  $Y_i$  and original functional covariates  $\mathbf{X}_i(t)$ , where  $\boldsymbol{\eta}(t) = (\eta_1(t), \dots, \eta_p(t))' = p^{-1} \mathbf{B} \Phi'(t) \alpha$  is the regression coefficient function. To visualize the coefficient function, we choose one ROI from each class in Table 2 and plot the corresponding

Table 2: The ROIs and their clusters.

| ROI            | name                             | ROI  | name                             | ROI  | name                             |
|----------------|----------------------------------|------|----------------------------------|------|----------------------------------|
| <b>Class 1</b> |                                  |      |                                  |      |                                  |
| 5              | left inferior lateral ventricle  | 18   | left amygdala                    | 91   | left basal forebrain             |
| 10             | left thalamus proper             | 24   | CSF                              | 92   | right basal forebrain            |
| 11             | left caudate                     | 28   | left ventral DC                  | 632  | cerebellar vermal lobules VIII-X |
| 12             | left putamen                     | 49   | right thalamus proper            | 1014 | left medial orbitofrontal        |
| 14             | 3rd ventricle                    | 50   | right caudate                    | 1026 | left rostral anterior cingulate  |
| 15             | 4th ventricle                    | 53   | right hippocampus                | 2002 | right caudal anterior cingulate  |
| 16             | Brain stem                       | 54   | right amygdala                   |      |                                  |
| 17             | left hippocampus                 | 60   | right ventral DC                 |      |                                  |
| 2012           | right lateral orbitofrontal      | 2014 | right medial orbitofronta        |      |                                  |
| 2023           | right posterior cingulate        |      |                                  |      |                                  |
| <b>Class 2</b> |                                  |      |                                  |      |                                  |
| 51             | right putamen                    | 1016 | left parahippocampal             | 1025 | left precuneus                   |
| 630            | cerebellar vermal lobules I-V    | 1017 | left paracentral                 | 1035 | left insula                      |
| 631            | cerebellar vermal lobules VI-VII | 1021 | left pericalcarine               | 2013 | right lingual                    |
| 1012           | left lateral orbitofrontal       | 1023 | left posterior cingulate         | 2017 | right paracentral                |
| 1013           | left lingual                     | 1024 | left precentral                  | 2021 | right pericalcarine              |
| 2025           | right precuneus                  | 2026 | right rostral anterior cingulate |      |                                  |
| <b>Class 3</b> |                                  |      |                                  |      |                                  |
| 4              | left lateral ventricle           | 1018 | left pars opercularis            | 2010 | right isthmus cingulate          |
| 6              | left cerebellum exterior         | 1019 | left pars orbitalis              | 2011 | right lateral occipital          |
| 7              | left cerebellum white matter     | 1020 | left pars triangularis           | 2015 | right mid-temporal               |
| 43             | right lateral ventricle          | 1022 | left postcentral                 | 2016 | right parahippocampal            |
| 45             | right cerebellum exterior        | 1027 | left rostral mid-frontal         | 2018 | right pars opercularis           |
| 46             | right cerebellum white matter    | 1028 | left superior frontal            | 2019 | right pars orbitalis             |
| 1002           | left caudal anterior cingulate   | 1029 | left superior parietal           | 2020 | right pars triangularis          |
| 1003           | left caudal mid-frontal          | 1030 | left superior temporal           | 2022 | right postcentral                |
| 1005           | left cuneus                      | 1031 | left supramarginal               | 2024 | right precentral                 |
| 1006           | left entorhinal                  | 1034 | left transverse temporal         | 2027 | right rostral mid-frontal        |
| 1007           | left fusiform                    | 2003 | right caudal mid- frontal        | 2028 | right superior frontal           |
| 1008           | left inferior parietal           | 2005 | right cuneus                     | 2029 | right superior parietal          |
| 1009           | left inferior temporal           | 2006 | right entorhinal                 | 2030 | right superior temporal          |
| 1010           | left isthmus cingulate           | 2007 | right fusiform                   | 2031 | right supramarginal              |
| 1011           | left lateral occipital           | 2008 | right inferior parietal          | 2034 | right transverse temporal        |
| 1015           | left mid-temporal                | 2009 | right inferior temporal          | 2035 | right insula                     |

estimated coefficient function  $\hat{\eta}_j(t)$  for  $\eta_j(t)$  in Figure 4(b), which shows that the estimated coefficient function  $\hat{\boldsymbol{\eta}}(t)$  fluctuates violently around a horizontal line. This inspires us to compute the cumulative term  $\boldsymbol{\beta} = \int \hat{\boldsymbol{\eta}}(t)dt$  to measure the effects of the ROIs on the re-

sponse. Furthermore, for each ROI  $j$ , we perform hypothesis testing  $\beta_j = 0$  based on 200 bootstrap samples to test the effect of ROI  $j$  on AD. As a result, we identify 41 significant ROIs, as displayed in Table 3. All the significant ROI effects are negative, which implies that brain atrophy is associated with AD and is consistent with previous studies (Double et al., 1996). For example, the following conclusions have been found for the 41 significant ROIs:

- Medial temporal lobe (ROI<sub>2015</sub>) atrophy was reported by [Fruijtier et al. \(2019\)](#) to be one of the three best validated neuroimaging biomarkers for AD.
- The tau protein is an indicator of the extent of neuronal damage, and its pathology was verified by [Solders et al. \(2022\)](#) to propagate in a prion-like manner along the LC-transentorhinal cortex (ROI<sub>1006</sub> and ROI<sub>2006</sub>) and white matter (ROI<sub>46</sub>) pathway.
- In addition, frontal lobe (ROI<sub>1003</sub>, ROI<sub>1028</sub>, ROI<sub>2003</sub> and ROI<sub>2027</sub>) atrophy is a prominent symbol of AD and can accelerate the lesions of AD. This was reported by [Simona et al. \(2016\)](#).
- The atrophy of the parietal lobe (ROI<sub>1008</sub> and ROI<sub>1029</sub>), insula (ROI<sub>2035</sub>) and hippocampus (ROI<sub>17</sub> and ROI<sub>53</sub>) was found to induce AD by [Foundas et al. \(1997\)](#). Moreover, from Table 3, we can see that the effect of the left hippocampus (ROI<sub>17</sub>) is larger than that of the right hippocampus (ROI<sub>53</sub>), which is consistent with the findings of [Philip et al. \(2021\)](#), which state that the atrophy of left hippocampus is more severe than that of the right hippocampus in AD patients.
- The predictive function of fusiform gyrus (ROI<sub>1007</sub>) atrophy at the early stage of AD has been reported by [Chang et al. \(2016\)](#). [Donovan et al. \(2014\)](#) indicated damage to the supramarginal gyrus (ROI<sub>1031</sub>) atrophy to the human visual system in AD patients.



- The associations of atrophy in the caudate nucleus (ROI<sub>50</sub>), pars triangularis (ROI<sub>1020</sub> and ROI<sub>2020</sub>), pars opercularis (ROI<sub>1018</sub> and ROI<sub>2018</sub>), and amygdala (ROI<sub>54</sub>) with AD have also been extensively reported in the literature, for example, [Pearce et al. \(1984\)](#); [Whitwell \(2010\)](#) and [Stéphane et al. \(2011\)](#).

Table 3: Estimates, SDs and  $p$  values of  $\beta = \int \eta(t)dt$  for the ADNI data, where  $\eta(t)$  is the regression coefficient function of the ROIs.

| ROI  | Estimate | SD     | $p$ value | ROI  | Estimate | SD     | $p$ value | ROI  | Estimate | SD     | $p$ value |
|------|----------|--------|-----------|------|----------|--------|-----------|------|----------|--------|-----------|
| 5    | -5.9829  | 1.9892 | 0.0026    | 1008 | -1.7920  | 0.6487 | 0.0057    | 2008 | -2.7590  | 0.7487 | 0.0002    |
| 14   | -4.0130  | 1.8183 | 0.0273    | 1009 | -3.8436  | 0.9955 | 0.0001    | 2009 | -4.8168  | 1.2551 | 0.0001    |
| 17   | -6.0605  | 1.6149 | 0.0002    | 1011 | -2.9302  | 0.8575 | 0.0006    | 2010 | -2.3420  | 0.8745 | 0.0074    |
| 28   | -9.3520  | 2.4988 | 0.0002    | 1018 | -3.4751  | 1.0386 | 0.0008    | 2015 | -3.1155  | 0.8163 | 0.0001    |
| 45   | -2.5556  | 0.7636 | 0.0008    | 1020 | -3.6396  | 0.9609 | 0.0002    | 2018 | -2.4459  | 0.7143 | 0.0006    |
| 46   | -3.1817  | 1.2945 | 0.0140    | 1028 | -1.6740  | 0.6912 | 0.0154    | 2019 | -1.7958  | 0.7866 | 0.0224    |
| 50   | -7.4244  | 3.1591 | 0.0188    | 1029 | -3.1541  | 0.8261 | 0.0001    | 2020 | -1.8009  | 0.6835 | 0.0084    |
| 53   | -4.9068  | 1.2157 | 0.0001    | 1030 | -4.1952  | 1.0764 | 0.0001    | 2022 | -1.2041  | 0.6140 | 0.0499    |
| 54   | -5.9669  | 1.7803 | 0.0008    | 1031 | -2.3494  | 0.6523 | 0.0003    | 2027 | -1.6122  | 0.6545 | 0.0138    |
| 60   | -10.1306 | 2.8457 | 0.0004    | 1034 | -3.1273  | 1.0865 | 0.0004    | 2030 | -3.2471  | 0.8374 | 0.0001    |
| 1003 | -3.4179  | 0.9363 | 0.0003    | 2003 | -2.6540  | 0.7662 | 0.0005    | 2031 | -2.7265  | 0.7388 | 0.0002    |
| 1005 | -1.8912  | 0.6732 | 0.0049    | 2005 | -1.7878  | 0.6582 | 0.0066    | 2034 | -2.0218  | 0.9236 | 0.0286    |
| 1006 | -6.9455  | 2.1871 | 0.0015    | 2006 | -2.8513  | 0.8757 | 0.0011    | 2035 | -1.7238  | 0.7776 | 0.0266    |
| 1007 | -2.9910  | 0.7921 | 0.0002    | 2007 | -3.1506  | 0.8217 | 0.0001    |      |          |        |           |

## 6 Discussion

In this paper, we propose FaFPCA to extract features from high-dimensional functional data. By building some moment equations, we estimate loadings, scores and eigenfunctions in closed form without rotation. We also establish the theoretical properties of the proposed estimator, including the convergence rate and asymptotic normality. The proposed FaFPCA approach has the following advantages. (1) Computational efficiency. With the proper rewriting of the FaFPCA model, we directly estimate loadings, scores and eigenfunc-

tions in closed form so that complicated and likely nonconvergent iterations can be avoided.

(2) Blessing of dimensionality. In high-dimensional FDA, the dimension of function  $p$  is a burden for estimation and inference. In contrast, FaFPCA provides functional principal analysis under the framework of a factor model; as a result, the dimensionality curse becomes dimensionality welfare, which is confirmed by Theorems 1-4 and simulation studies.

(3) Theoretical interpretability. We give the theoretical properties of FaFPCA and show the relation to the traditional high-dimensional factor model. (4) High prediction accuracy.

Since we use both the correlation among the high-dimensional functional variables and the dependence over time, the proposed FaFPCA approach has a higher prediction accuracy than the existing methods, which is confirmed by real data analysis and simulation studies.

Various extensions can be considered in the future. For example, we can extend linear FaFPCA to the generalized case for discrete functional data. However, the computational and the theoretical availability for a nonlinear framework are worthy of further investigation. In practice, the observations  $\mathbf{X}_i(t), i = 1, \dots, n$  may be serially dependent, such as those considered by Tavakoli et al. (2021) and Guo et al. (2022), it is interesting to extend FaFPCA to high-dimensional functional time series analysis. In addition, in the paper, we only consider the dimension reduction of high-dimensional functional data. The features captured by the factors are the most important directions concerning the information of high-dimensional functional covariates alone rather than under the supervision of the response. It is an important question on how to extract factors from high-dimensional functional covariates in the direction supervised by a response variable.

## Acknowledgements

The functional magnetic resonance imaging (fMRI) scans provided by ADNI database (<http://adni.loni.usc.edu/>). ADNI was launched in 2003 by the National Institute

on Aging, the National Institute of Biomedical Imaging and Bioengineering, the Food and Drug Administration, private pharmaceutical companies and non-profit organizations as a \$60 million and 5-year public–private partnership. The primary goal of ADNI was to test whether serial MRI, PET and other biological markers are useful in clinical trials of mild cognitive impairment (MCI) and early AD. The determination of sensitive and specific markers of very early AD progression is intended to aid researchers and clinicians to develop new treatments and monitor their effectiveness and estimate the time and cost of clinical trials. ADNI subjects aged 55–90 years old and from over 50 sites across the USA and Canada participated in the research; more detailed information is available at ([www.adni-info.org](http://www.adni-info.org)).

Data used in preparation of this article were obtained from the Alzheimer’s Disease Neuroimaging Initiative (ADNI) database ([adni.loni.usc.edu](http://adni.loni.usc.edu)). As such, the investigators within the ADNI contributed to the design and implementation of ADNI and/or provided data but did not participate in analysis or writing of this report. A complete listing of ADNI investigators can be found at: [http://adni.loni.usc.edu/wp-content/uploads/how\\_to\\_apply/ADNI\\_Acknowledgement\\_List.pdf](http://adni.loni.usc.edu/wp-content/uploads/how_to_apply/ADNI_Acknowledgement_List.pdf).

## References

- Ash, R. and Gardner, M. (1975). *Topics in stochastic processes*. Academic Press.
- Bai, J. (2003). Inferential theory for factor models of large dimensions. *Econometrica*, 71(1):135–171.
- Bai, J. and Liao, Y. (2013). Statistical inferences using large estimated covariances for panel data and factor models. *arXiv:1307.2662*.

- Bai, J. and Ng, S. (2002). Determining the number of factors in approximate factor models. *Econometrica*, 70(1):191–221.
- Bai, J. and Ng, S. (2006). Confidence intervals for diffusion index forecasts and inference for factor-augmented regressions. *Econometrica*, 74(4):1133–1150.
- Bai, J. and Ng, S. (2013). Principal components estimation and identification of static factors. *Journal of Econometrics*, 176(1):18–29.
- Chang, J., Chen, C., Qiao, X., and Yao, Q. (2020). An autocovariance-based learning framework for high-dimensional functional time series. *arXiv:2008.12885*.
- Chang, Y. T., Huang, C. W., Chen, N. C., Lin, K. J., Huang, S. H., Chang, W. N., Shih-Wei, H., Che-Wei, H., Chen, H. H., and Chang, C. C. (2016). Hippocampal amyloid burden with downstream fusiform gyrus atrophy correlate with face matching task scores in early stage alzheimer’s disease. *Frontiers in Aging Neuroence*, 8.
- Chiou, J.-M., Chen, Y.-T., and Yang, Y.-F. (2014). Multivariate functional principal component analysis: A normalization approach. *Statistica Sinica*, 24(4):1571–1596.
- Chiou, J.-M. and Müller, H.-G. (2014). Linear manifold modelling of multivariate functional data. *Journal of the Royal Statistical Society: Series B (Statistical Methodology)*, 76(3):605–626.
- Donovan, N. J., Wadsworth, L. P., Lorus, N., Locascio, J. J., Rentz, D. M., Johnson, K. A., Sperling, R. A., and Marshall, G. A. (2014). Regional cortical thinning predicts worsening apathy and hallucinations across the alzheimer disease spectrum. *American Journal of Geriatric Psychiatry*, 22(11):1168–1179.
- Double, K., Halliday, G., Krill, J., Harasty, J., Cullen, K., Brooks, W., Creasey, H., and

- Broe, G. (1996). Topography of brain atrophy during normal aging and alzheimer's disease. *Neurobiology of Aging*, 17(4):513–521.
- Fan, J., Liao, Y., and Mincheva, M. (2013). Large covariance estimation by thresholding principal orthogonal complements. *Journal of the Royal Statistical Society: Series B (Statistical Methodology)*, 75(4):603–680.
- Fang, Q., Guo, S., and Qiao, X. (2021). Finite sample theory for high-dimensional functional/scalar time series with applications. *arXiv:2004.07781*.
- Ferraty, F. and Vieu, P. (2006). *Nonparametric functional data analysis*. Springer.
- Foundas, A. L., Leonard, C. M., Mahoney, S. M., Agee, O. F., and Heilman, K. M. (1997). Atrophy of the hippocampus, parietal cortex, and insula in alzheimer's disease: A volumetric magnetic resonance imaging study. *Cognitive and Behavioral Neurology*, 10(2):81–89.
- Fruijtier, A. D., Visser, L., Maurik, I., Zwan, M., and Smets, E. (2019). Abide delphi study: topics to discuss in diagnostic consultations in memory clinics. *Alzheimer's Research and Therapy*, 11(1):77.
- Gao, Y., Shang, H. L., and Yang, Y. (2019). High-dimensional functional time series forecasting: An application to age-specific mortality rates. *Journal of Multivariate Analysis*, 170:232–243.
- Górecki, T., Krzyśko, M., Waszak, L., and Wołyński, W. (2018). Selected statistical methods of data analysis for multivariate functional data. *Statistical Papers*, 59(1):153–182.
- Grith, M., Wagner, H., Härdle, W. K., and Kneip, A. (2018). Functional principal component analysis for derivatives of multivariate curves. *Statistica Sinica*, 28(4):2469–2496.

- Guo, S. and Qiao, X. (2020). On consistency and sparsity for high-dimensional functional time series with application to autoregressions. *arXiv:2003.11462*.
- Guo, S., Qiao, X., and Wang, Q. (2022). Factor modelling for high-dimensional functional time series. *arXiv:2112.13651*.
- Hall, P. and Hosseini-Nasab, M. (2006). On properties of functional principal components analysis. *Journal of the Royal Statistical Society: Series B (Statistical Methodology)*, 68(1):109–126.
- Hall, P., Müller, H., and Yao, F. (2008). Modelling sparse generalized longitudinal observations with latent gaussian processes. *Journal of the Royal Statistical Society: Series B (Statistical Methodology)*, 70(4):703–723.
- Han, K., Müller, H.-G., and Park, B. U. (2018). Smooth backfitting for additive modeling with small errors-in-variables, with an application to additive functional regression for multiple predictor functions. *Bernoulli*, 24(2):1233–1265.
- Happ, C. and Greven, S. (2018). Multivariate functional principal component analysis for data observed on different (dimensional) domains. *Journal of the American Statistical Association*, 113(522):649–659.
- Happ, C., Scheipl, F., Gabriel, A.-A., and Greven, S. (2019). A general framework for multivariate functional principal component analysis of amplitude and phase variation. *Statistical Papers*, 8(e220):1–12.
- Horváth, L. and Kokoszka, P. (2012). *Inference for Functional Data with Applications*. Springer Science & Business Media.
- Hsing, T. and Eubank, R. (2015). *Theoretical Foundations of Functional Data Analysis, with an Introduction to Linear Operators*. John Wiley & Sons.

- Hu, X. and Yao, F. (2021). Dynamic principal subspaces in high dimensions. *arXiv:2104.03087*.
- Hu, X. and Yao, F. (2022). Sparse functional principal component analysis in high dimensions. *Statistica Sinica*, 38:1–22.
- Jacques, J. and Preda, C. (2014). Model-based clustering for multivariate functional data. *Computational Statistics and Data Analysis*, 71:92–106.
- James, G. M., Hastie, T. J., and Sugar, C. A. (2000). Principal component models for sparse functional data. *Biometrika*, 87(3):587–602.
- Jiang, F., Ma, Y., and Wei, Y. (2019). Sufficient direction factor model and its application to gene expression quantitative trait loci discovery. *Biometrika*, 106(2):417–432.
- Kokoszka, P. and Reimherr, M. (2017). *Introduction to Functional Data Analysis*. CRC Press.
- Kong, D., Xue, K., Yao, F., and Zhang, H. (2016). Partially functional linear regression in high dimensions. *Biometrika*, 103(1):147–159.
- Li, Q., Cheng, G., Fan, J., and Wang, Y. (2018). Embracing the blessing of dimensionality in factor models. *Journal of the American Statistical Association*, 113(521):380–389.
- Li, T., Zhu, H., Li, T., and Zhu, H. (2022). Asynchronous functional linear regression models for longitudinal data in reproducing kernel hilbert space. *Biometrics*, pages 1–16. <https://doi.org/10.1111/biom.13767>.
- Li, Y. and Hsing (2010). Deciding the dimension of effective dimension reduction space for functional and high-dimensional data. *The Annals of Statistics*, 38(5):3028–3062.
- Lian, H. (2013). Shrinkage estimation and selection for multiple functional regression. *Statistica Sinica*, 23(1):51–74.

- Lin, Z., Müller, H. G., and Yao, F. (2018). Mixture inner product spaces and their application to functional data analysis. *The Annals of Statistics*, 46(1):370–400.
- Liu, W., Lin, H., Zheng, S., and Liu, J. (2022+). Generalized factor model for ultra-high dimensional correlated variables with mixed types. *Journal of the American Statistical Association*, online.
- Mueller, S. G., Weiner, M. W., Thal, L. J., Petersen, R. C., Jack, C., Jagust, W., Trojanowski, J. Q., Toga, A. W., and Beckett, L. (2005). Alzheimer’s disease neuroimaging initiative. *Neuroimaging clinics of North America*, 15(4):869–877.
- Panaretos, V. M., Kraus, D., and Maddocks, J. H. (2010). Second-order comparison of gaussian random functions and the geometry of dna minicircles. *Journal of the American Statistical Association*, 105(490):670–682.
- Pearce, B. R., Palmer, A. M., Bowen, D. M., Wilcock, G. K., and Davison, A. N. (1984). Neurotransmitter dysfunction and atrophy of the caudate nucleus in alzheimer’s disease. *Neurochemical Pathology*, 2(4):221–232.
- Philip, S., Bart, D. S., Miia, K., Henne, H., Gael, C., Charlotte, E. T., Jeffrey, C., and Wiesje, M. v. d. F. (2021). Alzheimer’s disease. *Cognitive and Behavioral Neurology*, 397:1577–1590.
- Ramsay, J. O. (1982). When the data are functions. *Psychometrika*, 47(4):379–396.
- Ramsay, J. O. and Silverman, B. W. (2002). *Applied Functional Data Analysis*. Springer.
- Ramsay, J. O. and Silverman, B. W. (2005). *Functional Data Analysis*. Springer.
- Rice, J. A. and Silverman, B. W. (1991). Estimating the mean and covariance structure nonparametrically when the data are curves. *Journal of the Royal Statistical Society: Series B (Statistical Methodological)*, 53(1):233–243.



- Simona, S., Philip, S. I., Susanne, M., Duygu, T., Niklas, M., Clifford, R., Charles, D., Ronald, P., Paul, S. A., Weiner, M. W., ScottMackin, R., and Initiative, A. D. N. (2016). Chronic depressive symptomatology in mild cognitive impairment is associated with frontal atrophy rate which hastens conversion to alzheimer dementia. *American Journal of Geriatric Psychiatry*, 24(2):126–135.
- Solders, S. K., Galinsky, V. L., Clark, A. L., Sorg, S. F., Weigand, A. J., Bondi, M. W., and Frank, L. R. (2022). Diffusion mri tractography of the locus coeruleus-transentorhinal cortex connections using go-esp. *Magnetic Resonance in Medicine*, 87:1816–1831.
- Solea, E. and Dette, H. (2021). Nonparametric and high-dimensional functional graphical models. *arXiv:2103.10568*.
- Stone, C. J. (1980). Optimal rates of convergence for nonparametric estimators. *The Annals of Statistics*, 8(6):1348–1360.
- Stéphane, P. P., Dautoff, R., Morris, J. C., Barrett, L. F., and Dickerson, B. C. (2011). Amygdala atrophy is prominent in early alzheimer’s disease and relates to symptom severity. *Psychiatry Research*, 194(1):7–13.
- Tang, C., Shang, H. L., and Yang, Y. (2021). Multi-population mortality forecasting using high-dimensional functional factor models. *arXiv:2109.04146*.
- Tang, C. and Shi, Y. (2021). Forecasting high-dimensional financial functional time series: An application to constituent stocks in dow jones index. *Journal of Risk and Financial Management*, 14(8):343.
- Tavakoli, S., Nisol, G., and Hallin, M. (2021). High-dimensional functional factor models. *arXiv:1905.10325*.

- Whitwell, J. L. (2010). Progression of atrophy in alzheimer’s disease and related disorders. *Neurotoxicity Research*, 18(3-4):339–346.
- Wong, R. K. W., Li, Y., and Zhu, Z. (2019). Partially linear functional additive models for multivariate functional data. *Journal of the American Statistical Association*, 114(525):406–418.
- Yao, F., Müller, H.-G., and Wang, J.-L. (2005). Functional data analysis for sparse longitudinal data. *Journal of the American Statistical Association*, 100(470):577–590.
- Zhao, B., Ibrahim, J. G., Li, Y., Li, T., Wang, Y., Shan, Y., Zhu, Z., Zhou, F., Zhang, J., Huang, C., Liao, H., Yang, L., Thompson, P. M., and Zhu, H. (2019). Heritability of regional brain volumes in large-scale neuroimaging and genetic studies. *Cerebral Cortex*, 29(7):2904–2914.
- Zhong, Q., Lin, H., and Li, Y. (2021). Cluster non-gaussian functional data. *Biometrics*, 77(3):852–865.
- Zhou, L., Lin, H., and Liang, H. (2018). Efficient estimation of the nonparametric mean and covariance functions for longitudinal and sparse functional data. *Journal of the American statistical association*, 113(524):1550–1564.
- Zhu, H., Strawn, N., and Dunson, D. B. (2016). Bayesian graphical models for multivariate functional data. *The Journal of Machine Learning Research*, 17(1):7157–7183.